IOP Publishing Journal of Physics: Condensed Matter
J. Phys.: Condens. Matter **28** (2016) 126004 (6pp) doi:10.1088/0953-8984/28/12/126004

Graphene-based half-metal and spin-semiconductor for spintronic applications

Jingshan Qi[1,4], Xiaofang Chen[1], Kaige Hu[2,3] and Ji Feng[2,3]

[1] School of Physics and Electronic Engineering, Jiangsu Normal University, Xuzhou 221116, People's Republic of China
[2] International Center for Quantum Materials, School of Physics, Peking University, Beijing 100871, People's Republic of China
[3] Collaborative Innovation Center of Quantum Matter, Beijing 100871, People's Republic of China
[4] Key Laboratory for Intelligent Nano Materials and Devices of the Ministry of Education, Nanjing 210016, People's Republic of China

E-mail: qijingshan@jsnu.edu.cn and hukaige@pku.edu.cn

Received 27 October 2015, revised 9 January 2016
Accepted for publication 1 February 2016
Published 2 March 2016

Abstract

In this letter we propose a strategy to make graphene become a half-metal or spin-semiconductor by combining the magnetic proximity effects and sublattice symmetry breaking in graphone/graphene and graphone/graphene/BN heterostructures. Exchange interactions lift the spin degeneracy and sublattice symmetry breaking opens a band gap in graphene. More interestingly, the gap opening depends on the spin direction and the competition between the sublattice asymmetry and exchange field determines the system is a half-metal or a spin-semiconductor. By first-principles calculations and a low-energy effective model analysis, we elucidate the underlying physical mechanism of spin-dependent gap opening and spin degeneracy splitting. This offers an alternative practical platform for graphene-based spintronics.

Keywords: heterostructure, magnetism, graphene, spintronics

(Some figures may appear in colour only in the online journal)

A spintronic device uses spins instead of charge as information carriers [1, 2]. 2D graphene has demonstrated long spin diffusion lengths up to room temperature [3]. This offers an unprecedented platform for spintronics, in which a complete integration of spin injection, manipulation, and detection could lead to ultra-fast electronic circuits. However, a fundamental challenge lies in the development of external ways to control the propagation of spin-polarized currents at room temperature [4, 5].

Spins in graphene can be influenced by the presence of local magnetic ordering intentionally generated by the material design. For instance, edge magnetism has been shown to develop in ultra-narrow graphene nanoribbons (GNRs) for certain edge geometries [6, 7]. It is well known that a GNR with straight zigzag edges has an antiferromagnetic (AFM) ground state [8]. First-principles calculations predicted that, under a transverse electrical field, the zigzag GNR becomes a half-metal [6], in which the carriers are 100% spin polarized with only one spin state conducting. Another interesting example is a spin semiconductor [9], or a spin gapless semiconductor [10–14], in which each spin state has a gap but is relatively energy shifted, so that the carriers are also 100% spin polarized with either electrons conducting one spin or the holes conducting the other. Wang *et al* proposed the realization of a spin semiconductor in graphene nanoribbons with sawtooth zigzag edges by first-principles calculations [9]. However, ultra-narrow nanoribbons with certain edge geometries will encounter serious issues with fabrication in practice. There is also a lot of interest currently devoted to developing magnetism in graphene by depositing or doping metal atoms. Unfortunately, magnetic interactions between dopants usually change with their distance, which is not well

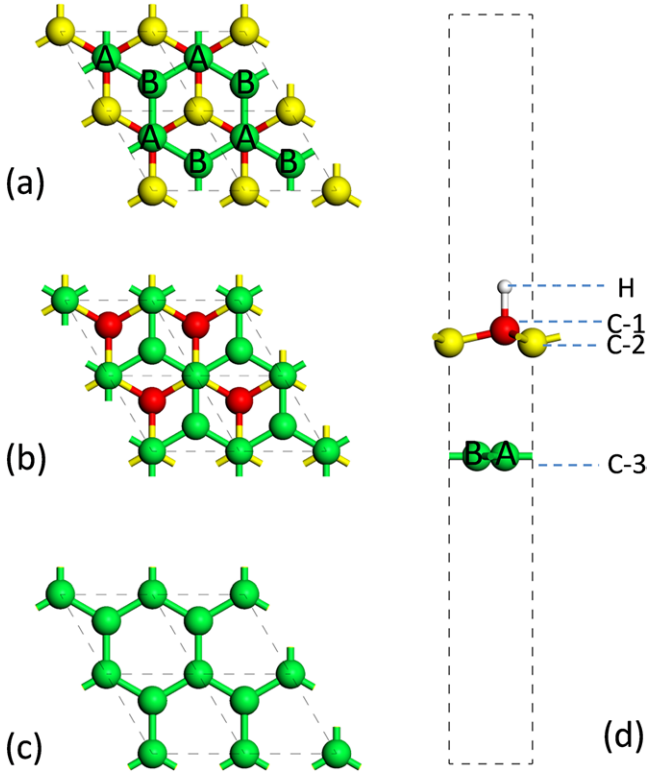

Figure 1. Three typical graphone/graphene systems with different stacking orders between graphene and graphone. (a) Top view of the AB-I configuration. C-2 is on the hexagonal hole of graphene. (b) Top view of the AB-II configuration. C-1 is on the hexagonal hole of graphene. (c) Top view of the AA configuration. Both C-1 and C-2 are positioned exactly above C-3. (d) Side view of the AB-I configuration. The sublattices are marked by the letters A and B, respectively.

controlled in realistic samples. In addition, scattering caused by random impurities could be detrimental to its high carrier mobility, a unique electronic property that is better to be preserved. Furthermore, the growth of graphene on magnetic metal [15–18] and insulator [19, 20] substrates was also proposed as a route to tailor graphene spin properties. Yang *et al* reported by first-principles calculations that the proximity of a magnetic insulator EuO will induce a strong spin polarization in graphene and a band gap at the Dirac point with an exchange splitting of 36 meV [21]. This is important progress in graphene-based spintronics, though the low cure temperature of EuO limits its practical application at room temperature. There is still a lot of effort underway to explore novel materials or practical controlling methods in spintronics.

In this letter we report that graphene can become a half-metal or spin semiconductor by combining magnetic proximity effects and symmetry breaking. Our system can be fabricated by single-side semihydrogenating a bilayer graphene, i.e. only one sublattice of one of the two layers is hydrogenated, as shown in figure 1. This system can also be seen to be composed of a graphene sheet and a single-side semihydrogenated graphene sheet termed graphone [22]. Since graphone is a ferromagnetic semiconductor with a high Curie temperature and magnetic moments localized at the unhydrogenated carbon atoms [22], a foreign magnetic substrate is not needed to introduce exchange fields. First-principles calculations are carried out in the framework of the generalized gradient approximation of Perdew–Burke–Ernzerhof for the exchange–correlation functionals [23] using the Vienna *ab initio* simulation package [24]. A vacuum layer of 20 Å is used to ensure decoupling between neighboring slabs. All self-consistent calculations were performed with a plane wave cut-off of 500 eV on a $45 \times 45 \times 1$ Monkhorst–Pack k-point mesh. For structural relaxations, all the atoms are allowed to relax until the atomic forces are smaller than 0.001 eV Å^{-1}. To describe the van der Waals-type interaction between graphene and graphone, we employed a semi-empirical correction using Grimme's method [25]. We also carried out calculations with the spin–orbit coupling. No significant difference was found, indicating that the spin–orbit coupling effect is negligible.

The graphone/graphene system is a metastable state, energetically higher than a reconstructed interlayer-bonded configuration by 1.96 eV supercell^{-1} [26]. However, along the reaction pathway there is a very high-energy barrier of 1.83 eV supercell^{-1} [26], making this configuration stable at room temperature. The calculated lattice constants of graphene and graphone are 2.468 Å and 2.536 Å, respectively, a lattice mismatch of 2.7%. In the following, we evaluate the stability of the graphone/graphene system with different stacking orders between graphone and graphene. In graphone the hydrogenated carbons are marked C-1 and the unhydrogenated carbon atoms are marked C-2, as shown in figure 1. The carbons in graphene are marked C-3. We consider three typical stacking orders. The first is that C-2 is on the hexagonal holes of graphene, which we refer to as the AB-I configuration, as shown in figure 1(a). The second is that C-1 is on the hexagonal holes of graphene, which we refer to as the AB-II configuration, as shown in figure 1(b). The third is that both C-1 and C-2 are positioned exactly above C-3, which we refer to as the AA configuration, as shown in figure 1(c). Energetically, the AB-I configuration is more favorable than the AB-II and AA configurations by 10 meV and 8 meV cell^{-1}, respectively. Figure 1(d) shows the side view of the AB-I configuration. The distance between the C-2 and C-3 layers is 3.045 Å, less than the interlayer distance of graphite, indicating the stronger interaction between them. The interlayer binding energy is 0.136 eV unit cell^{-1}, larger than that of the bilayer graphene, 0.101 eV unit cell^{-1}.

In the following, we calculate the band structure and density of states (DOS) of the most stable AB-I configuration. From the projected DOS (PDOS) in figure 2(b), we can see that the states closest to the Fermi energy level are from graphene, i.e. C-3 atoms. There is a strong peak of the polarized C-p_z state from C-2 around the Fermi energy level. Spin-polarized π orbitals in graphone induce exchange interactions in the adjacent graphene. Exchange interactions lift the spin degeneracy of graphene and thus make spin-up and spin-down bands cross each other, as shown in figure 2(a). The spin-up and spin-down band structures are indicated by red and blue curves, respectively. In addition, the linear dispersion of the graphene band structure is also modified, with a gap opening at the K point due to sublattice symmetry breaking in graphene. More interestingly, this degeneracy lifting is spin

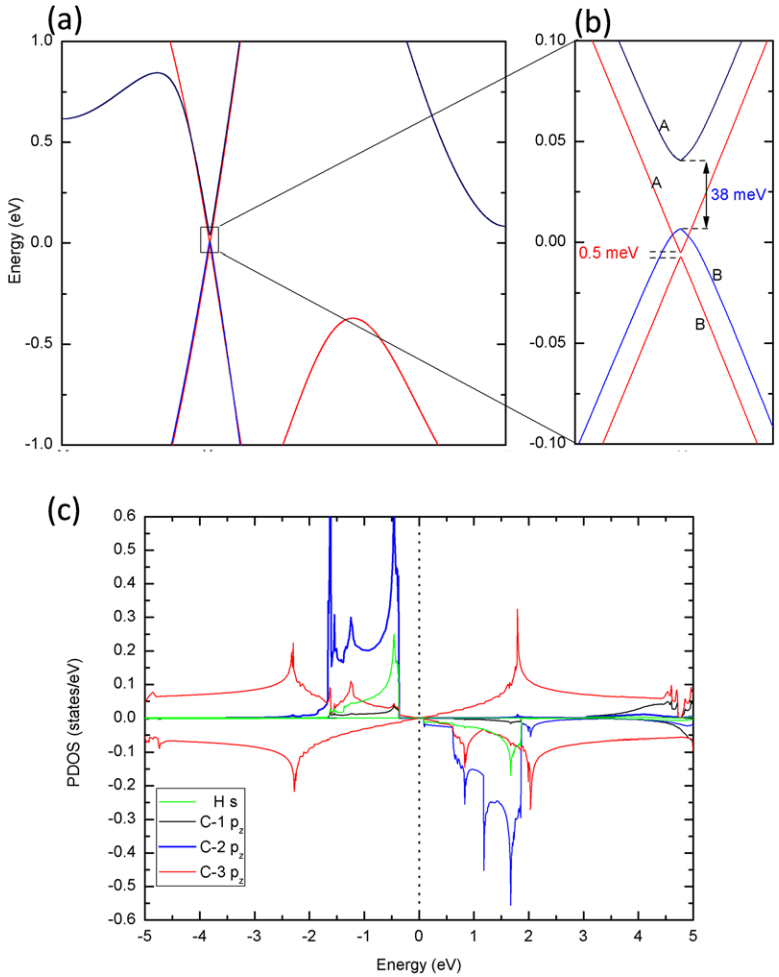

Figure 2. (a) The band structures, (b) the amplified view near the Fermi level, and (c) the PDOS of the most stable AB-I configuration.

dependent. The gap width is 0.5 meV for the spin-up bands and 38 meV for the spin-down bands, respectively. As a result, there is a 33 meV energy window, where the current would be 100% spin-polarized (half-metal) when the Fermi level lies in this energy window.

If we further break the sublattice symmetry of the graphene lattice, another interesting phenomenon will happen, i.e. a larger gap can be opened at the K (or K') point. When the gap is larger than the exchange splitting, the graphene sheet will become a spin semiconductor. For this purpose, we put the graphone/graphene sheet on a substrate of hexagonal boron nitride (BN), with graphene contacting the substrate. The calculated lattice constant of the BN monolayer is 2.513 Å, indicating a lattice mismatch of 1.8% between BN and graphene. We first study the stacking order between the BN substrate and graphene. Because the sublattice symmetry of graphene is broken by graphone, the two sublattices in graphene are no longer equivalent to each other, therefore we refer to the corresponding C atoms as *A*-sites and *B*-sites, as shown in figure 3. There are six typical stacking orders between BN and graphene due to the sublattice asymmetry of graphene. The first class is that the *A*-sites (*B*-sites) in graphene are positioned exactly above the B atoms, and the *B*-sites (*A*-sites) are on the hexagonal holes of the BN lattice, which we refer to as the ABC-I class. The second class is that the *A*-sites (*B*-sites) in graphene are positioned exactly above the N atoms, and the *B*-sites (*A*-sites) are on the hexagonal holes of the BN lattice, which we refer to as the ABC-II class. The third class is that the B and N atoms are, respectively, positioned exactly above the *A*-sites and *B*-sites (*B*-sites and *A*-sites) of graphene, which we refer to as the ABB class. First-principles total-energy calculations indicate that the ABC-I class is more favorable than the other configurations by more than 27 meV unit cell^{-1}. The ABC-I class actually includes two possible configurations, as shown in figure 3, which are nearly degeneracy in energy (<1 meV unit cell^{-1}). One configuration is that the *B*-sites in graphene are positioned exactly above the B atoms (see figures 3(a) and (b)), which we refer to as the ABC-Ia configuration; the other is that the *A*-sites in graphene are positioned exactly above the B atoms (see figures 3(c) and (d)), which we refer to as the ABC-Ib configuration. The distance between graphene and the BN layer is 3.129 Å. The interlayer binding energy between BN and graphene/graphone is 0.128 eV unit cell^{-1}, less than that between graphene and graphone, and larger than that between bilayer graphene.

In the following, we calculate the band structures of the two most stable ABC-I configurations. The BN substrate further induces sublattice asymmetry in grapheme, and thus opens a larger band gap than the graphone/graphene system at the K point, as shown in figure 4. Therefore, graphene

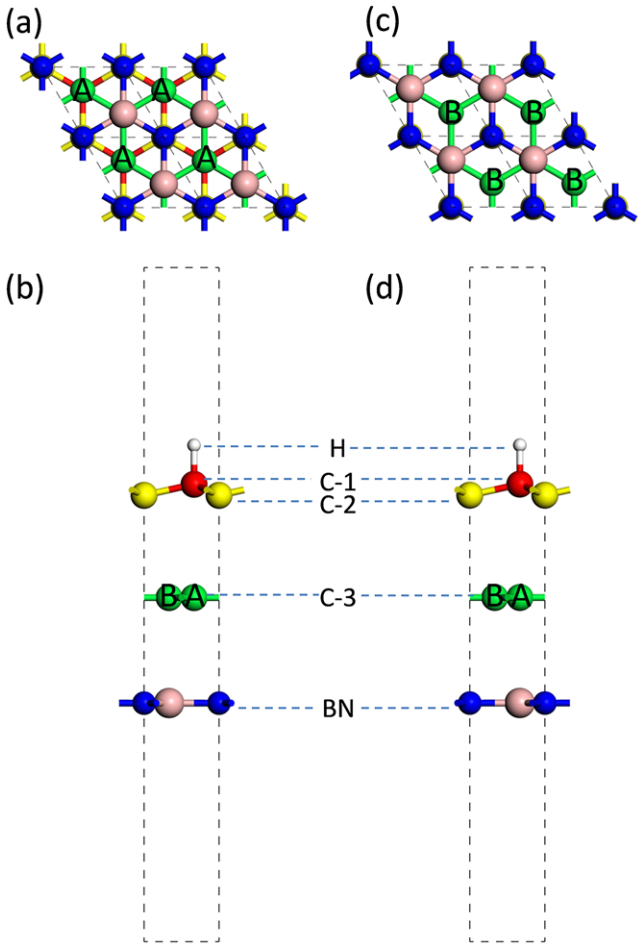

Figure 3. The two most stable stacking configurations between BN and graphene. (a) and (b) are the top view and side view of the ABC-Ia configuration, respectively. (c) and (d) are the top view and side view of the ABC-Ib configuration, respectively. The sublattices are marked by the letters A and B, respectively.

becomes a spin semiconductor, in which each spin has a gap but is relatively energy shifted, so that the carriers are 100% spin polarized with either electrons conducting one spin or holes conducting the other spin. The gap is larger than that of graphene/graphone and is also spin dependent. For the ABC-Ia configuration, the gap is 72 meV for the spin-up bands and 108 meV for the spin-down bands (see figure 4(a)), respectively. The system becomes a semiconductor with a direct gap of 59 meV. For the ABC-Ib configuration, the gap is 70 meV for the spin-up bands and 34 meV for the spin-down bands, respectively. This system is also a semiconductor with a direct gap of 21 meV. If we further tune the Fermi level by a gate voltage, either electrons or holes can be used as charge carriers for transport, but with opposite spins. This spin tunable feature can be very useful to design spintronic devices.

It is evident that the proximity-induced interactions lead to exchange splitting and gap opening. In the following, a low-energy effective Hamiltonian (LEH) [27, 28] is constructed to understand the spin-dependent gap opening caused by these interactions. The LEH can be expressed as $H = H_0 + H_m + H_{ex}$, with

$$H_0 = v_F(k_x\sigma_x + k_y\sigma_y)s_0,$$
$$H_m = \frac{m}{2}\sigma_z s_0,$$
$$H_{ex} = -(M_A\sigma_+ + M_B\sigma_-)s_z,$$

where H_0 is the Hamiltonian for the pristine graphene, v_F is the Fermi velocity. s_i and σ_i $(i = x, y, z, 0)$ are the Pauli matrices referring to the real spin and the orbital pseudospin, respectively, and $\sigma_\pm = \frac{1}{2}(\sigma_0 \pm \sigma_z)$. The band structure is shown in figure 5(a), where the Dirac cone and linear dispersion relation are well known. H_m is the mass term opening a gap in graphene due to the sublattice symmetry breaking from interactions with the adjacent materials, i.e. graphone and BN. When only $H_0 + H_m$ is considered, graphene becomes a semiconductor with spin degeneracy, as shown in figure 5(b). For the graphone/graphene system, the gap opening is due to the AB sublattice on-site potential energy difference induced by graphone (see figures 1(a) and (d)). The on-site energy of the electrons at the *A*-sites is higher than that at the *B*-sites. Therefore, the conduction bands and valence bands are contributed by the *A*-sites and *B*-sites, respectively, as shown in figure 2(b). For graphone/graphene/BN systems, the gap opening is contributed by graphone on one side and BN on the other side. Due to different stacking configurations between graphene and BN, the two contributions from graphone and BN can be enhanced or weakened by each other. For the ABC-Ia configuration, the B atoms are positioned to the *B*-sites. This decreases the on-site potential energy of the electrons on the *B*-sites. Therefore, the two contributions are enhanced by each other, widening the gap. For the ABC-Ib configuration, the B atoms are positioned to the *A*-sites and thus the two contributions are weakened by each other, narrowing the gap.

H_{ex} represents the exchange magnetization from the adjacent graphone. Due to the sublattice asymmetry, the exchange fields felt by the electrons on the *A*-sites and *B*-sites are different. Therefore, in H_{ex} we use M_A and M_B to represent the different exchange interactions for the valence and conduction bands, respectively. Exchange interactions lead to relative movement and intersect between the spin subbands, which makes the graphone/graphene system become a metal (see figure 5(c)) and the graphone/graphene/BN system a spin semiconductor (figures 5(d) and (e)). Due to different values of M_A and M_B, the movement of the valence and con duction bands of the same spin is also different. The fitted values according to the first-principles results are$m = 19.2$ meV, $M_A = 26.5$ meV, and$M_B = 7.7$ meV for the graphone/graphene C-I configuration. For the graphone/graphene/BN ABC-Ia configuration, the fitted values are$m = 90$ meV, $M_A = 24.5$ meV, and $M_B = 6.5$ meV. For the ABC-Ib configuration, the fitted values are $m = -52$ meV, $M_A = 24.5$ meV, and $M_B = 6.5$ meV. We can see that the exchange fields (M_A and M_B) are almost the same for those systems because the exchange fields are supplied uniquely by graphone. In addition, the contribution to the gap from graphone is 19.2 meV. The contribution from BN can be calculated from the m values of C-I and ABC-Ia, i.e. $90 - 19.2 = 70.8$ meV. The

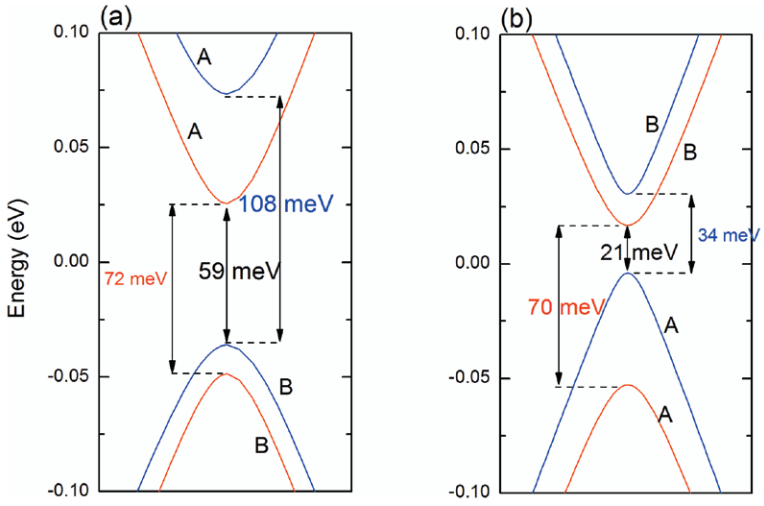

Figure 4. Band structures of (a) the ABC-Ia configuration and (b) the ABC-Ib configuration.

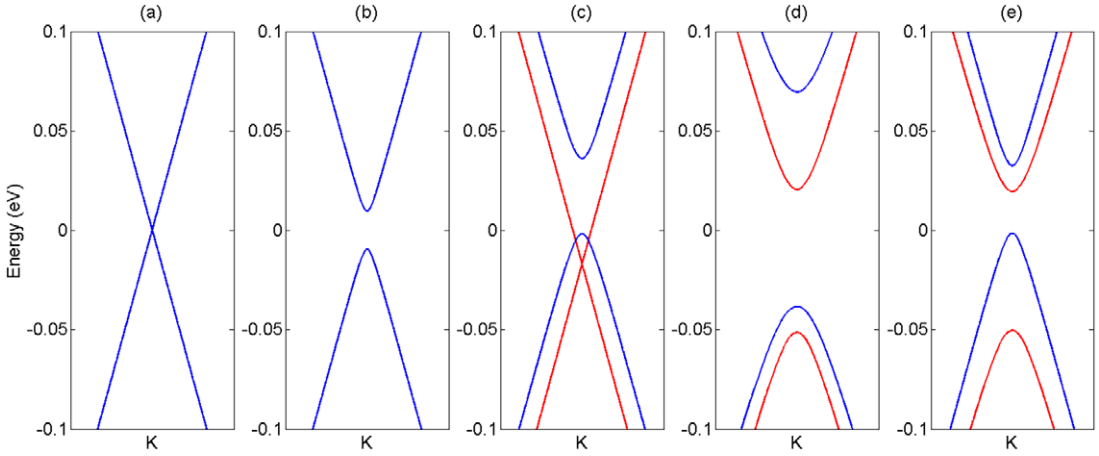

Figure 5. Band structures of graphene from the LEH model at different parameter values: (a) $m = 0$, $M_A = 0$ and $M_B = 0$; (b) $m = 19.2$ meV, $M_A = 0$ and $M_B = 0$; (c) $m = 19.2$ meV, $M_A = 26.5$ meV and $M_B = 7.7$ meV; (d) $m = 90$ meV, $M_A = 24.5$ meV and $M_B = 6.5$ meV; (e) $m = -52$ meV, $M_A = 24.5$ meV and $M_B = 6.5$ meV.

contribution can be also calculated from the m values of C-I and ABC-Ib, i.e. $-52 - 19.2 = -71.2$ meV. The opposite signs indicate the opposite contributions from BN to the AB sublattice on-site potential energy difference of graphene. The almost equal absolute values also indicate the contribution of BN to the gap opening is stable and about 71 meV. Therefore, the LEH reveals the importance of exchange fields and sublattice symmetry breaking induced by the adjacent materials and well elucidates the underlying physical mechanism of spin-dependent gap opening and spin degeneracy splitting. This LEH should be applicable to other graphene-based materials with exchange fields and sublattice symmetry breaking. Depending on the details of the materials, these parameters m, M_A and M_B will be different and thus the properties could also be different. For example, the spin gapless semiconductor can be obtained with suitable parameters.

Finally, we must point out that the role of the BN substrate is to open a larger gap in graphene. Although the natural 1.8% mismatch between the graphene and BN lattices leads to a moire pattern, not considered in our first principles calculations, a band gap is indeed observed in a heterostructure consisting of a graphene and BN [29]. In addition, we also check the effect of the lattice mismatch on the magnetism of graphone. We find that the magnetism of graphone is basically not influenced in the strain range from -3% to 3%. So, our proposed strategy is still applicable to the practical graphone/graphene/BN heterostructures.

In conclusion, by first-principles calculations we proposed a strategy to make graphene become a half-metal or spin semiconductor by combining exchange interactions and sublattice symmetry breaking in graphone/graphene and graphone/graphene/BN systems. The physical mechanism of spin-dependent gap opening and spin degeneracy splitting is well elucidated by a LEH model analysis. These designed materials offer an alternative practical platform for graphene-based spintronics.

Acknowledgments

We acknowledge the financial support from the National Natural Science Foundation of China (Projects No. 11204110, 11347005, 11174009), the China 973 Program (Projects No.

2013CB921900 and No. 2012CB921300), PAPD and the Open Fund of Key Laboratory for Intelligent Nano Materials and Devices of the Ministry of Education No. INMD-2015M04.

References

[1] Žutić I, Fabian J and Das Sarma S 2004 *Rev. Mod. Phys.* **76** 323
[2] Wolf S A, Awschalom D D, Buhrman R A, Daughton J M, von Molnár S, Roukes M L, Chtchelkanova A Y and Treger D M 2001 *Science* **294** 1488
[3] Han W, Kawakami R K, Gmitra M and Fabian J 2014 *Nat. Nano* **9** 794
[4] Das Sarma S, Adam S, Hwang E H and Rossi E 2011 *Rev. Mod. Phys.* **83** 407
[5] Semenov Y G, Kim K W and Zavada J M 2007 *Appl. Phys. Lett.* **91** 153105
[6] Son Y-W, Cohen M L and Louie S G 2006 *Nature* **444** 347
[7] Kim W Y and Kim K S 2008 *Nat. Nano* **3** 408
[8] Magda G Z, Jin X, Hagymasi I, Vancso P, Osvath Z, Nemes-Incze P, Hwang C, Biro L P and Tapaszto L 2014 *Nature* **514** 608
[9] Wang Z F, Jin S and Liu F 2013 *Phys. Rev. Lett.* **111** 096803
[10] Wang X L 2008 *Phys. Rev. Lett.* **100** 156404
[11] Li Y, Zhou Z, Shen P and Chen Z 2009 *ACS Nano* **3** 1952
[12] Pan Y and Yang Z 2010 *Phys. Rev.* B **82** 195308
[13] Hu X, Zhang W, Sun L and Krasheninnikov A V 2012 *Phys. Rev.* B **86** 195418
[14] Skaftouros S, Özdoğan K, Şaşıoğlu E and Galanakis I 2013 *Appl. Phys. Lett.* **102** 022402
[15] Giovannetti G, Khomyakov P A, Brocks G, Karpan V M, van den Brink J and Kelly P J 2008 *Phys. Rev. Lett.* **101** 026803
[16] Rader O, Varykhalov A, Sánchez-Barriga J, Marchenko D, Rybkin A and Shikin A M 2009 *Phys. Rev. Lett.* **102** 057602
[17] Varykhalov A, Sánchez-Barriga J, Shikin A M, Biswas C, Vescovo E, Rybkin A, Marchenko D and Rader O 2008 *Phys. Rev. Lett.* **101** 157601
[18] Weser M, Rehder Y, Horn K, Sicot M, Fonin M, Preobrajenski A B, Voloshina E N, Goering E and Dedkov Y S 2010 *Appl. Phys. Lett.* **96** 012504
[19] Haugen H, Huertas-Hernando D and Brataas A 2008 *Phys. Rev.* B **77** 115406
[20] Swartz A G, Odenthal P M, Hao Y, Ruoff R S and Kawakami R K 2012 *ACS Nano* **6** 10063
[21] Yang H X, Hallal A, Terrade D, Waintal X, Roche S and Chshiev M 2013 *Phys. Rev. Lett.* **110** 046603
[22] Zhou J, Wang Q, Sun Q, Chen X S, Kawazoe Y and Jena P 2009 *Nano Lett.* **9** 3867
[23] Perdew J P, Burke K and Ernzerhof M 1996 *Phys. Rev. Lett.* **77** 3865
[24] Kresse G and Hafner J 1993 *Phys. Rev.* B **47** 558
[25] Grimme S 2006 *J. Comput. Chem.* **27** 1787
[26] Zhou J, Wang Q, Sun Q and Jena P 2011 *Appl. Phys. Lett.* **98** 063108
[27] Kane C L and Mele E J 2005 *Phys. Rev. Lett.* **95** 226801
[28] Xiao D, Yao W and Niu Q 2007 *Phys. Rev. Lett.* **99** 236809
[29] Hunt B *et al* 2013 *Science* **340** 1427